Title

DEVELOPMENT OF ANODES FOR ALUMINUM/AIR BATTERIES - SOLUTION PHASE INHIBITION OF CORROSION

Authors

Macdonald, D.D.
English, C.
Urquidi-Macdonald, M.

Publication Date

1989-03-01

LBL-26999 c.2
UC-210

Lawrence Berkeley Laboratory
UNIVERSITY OF CALIFORNIA

APPLIED SCIENCE DIVISION

Development of Anodes for Aluminum/Air Batteries—Solution Phase Inhibition of Corrosion

Final Report

D.D. Macdonald, C. English, and M. Urquidi-Macdonald

March 1989

APPLIED SCIENCE DIVISION

Prepared for the U.S. Department of Energy under Contract Number DE-AC03-76SF00098.

DISCLAIMER

LBL-26999

DEVELOPMENT OF ANODES FOR ALUMINUM/AIR BATTERIES — SOLUTION PHASE INHIBITION OF CORROSION

Final Report

March 1989

by

Digby D. Macdonald
Catherine English
Mirna Urquidi-Macdonald

Department of Chemistry
SRI International
333 Ravenswood Avenue
Menlo Park, California 94025

for

Technology Base Research Project
Applied Science Division
Lawrence Berkeley Laboratory
1 Cyclotron Road
Berkeley, California 94720

This work was supported by the Assistant Secretary for Conservation and Renewable Energy, Office of Energy Storage and Distribution, Energy Storage Division of the U.S. Department of Energy under Contract No. DE-AC03-76SF00098, Subcontract No. 4550810 with the Lawrence Berkeley Laboratory.

EXECUTIVE SUMMARY

Solution-phase inhibition is a promising strategy for controlling the corrosion of the aluminum fuel in alkaline aluminum/air batteries. Development of effective inhibitors would permit the use of scrap aluminum as fuel and thereby significantly improve the economics of the battery, because the cost of the fuel would have been partly or wholly defrayed by its previous use.

In this study, we explored the discharge characteristics of aluminum in inhibited and uninhibited 4 M KOH at 50°C and compared the performance of the fuel with that for two leading alloy fuels that had been evaluated in our previous work, Alloy BDW (Al-1Mg-0.1In-0.2Mn) and Alloy 21 (Al-0.2Ga-0.1In-0.1Tl). The inhibitors employed in this study, SnO_3^{2-}, $In(OH)_3$, $Ga(OH)_4^-$, MnO_4^{2-}, and binary combinations thereof, are either alloying elements of Alloys BDW and 21 or have been investigated previously (SnO_3^{2-}), albeit in bench-scale test cells and not at the fundamental level.

We found that potassium manganate (K_2MnO_4) and $Na_2SnO_3 + In(OH)_3$ are effective inhibitor systems, particularly at high discharge rates (400 mA/cm^2), but at low discharge rates only manganate offers a significant advantage in coulombic efficiency over the uninhibited solution. Alloy BDW exhibits a very low open circuit (standby) corrosion rate, but its coulombic efficiency under discharge, as determined by delineating the partial anodic and cathodic reactions, was found to be no better than that of aluminum in the same uninhibited solution. Alloy 21 was found to exhibit a comparable performance to Alloy BDW under open circuit conditions and a much higher coulombic efficiency at low discharge rates (100 mA/cm^2), but the performance of this alloy under high discharge rate conditions was not determined. Alloy 21 has the significant disadvantage that it contains thallium.

CONTENTS

FIGURES

INTRODUCTION

Aluminum/air batteries are currently being developed for vehicular propulsion and as primary power sources for some stationary applications.[1-24] Regardless of the nature of the electrolyte (acidic, neutral, or alkaline), these primary cells consist of an aluminum alloy anode and a unifunctional air cathode. The advantages this system offers over other metal/air batteries (e.g., Fe/air, Zn/air) are the very high theoretical energy density of the fuel,[15] the unifunctional mode of operation of the air cathode (which ensures a longer life than that of the bifunctional counterpart), and the fact that the system is mechanically rather than electrically recharged. This latter feature is particularly important, because it should be possible to refuel an aluminum/air battery in a time comparable to that for an internal combustion engine (ICE), which is only a small fraction of that for electrically recharged (secondary) batteries such as Fe/air and Zn/air. Accordingly, Al/air batteries (or fuel cells) are more suited to long-range, multiple refueling operations than to short intracity excursions. The benign nature of the fuel and the near-ambient temperature of operation also render Al/air batteries suitable for some military and reserve applications.

To a large extent, the performance of an Al/air battery is determined by the electrochemistry and corrosion properties of the fuel. Pure aluminum is too reactive to be used directly, particularly in the highly alkaline electrolytes required for optimal performance of the air cathode. Consequently, considerable work has been reported on the development of dilute alloy fuels that have superior corrosion resistance under open circuit (standby) conditions and have acceptable discharge characteristics (see References 22 and 24 and the references therein). Several promising alloys have been developed,[22,24] but they are of limited practical application because they either contain toxic alloying elements (e.g., Tl) or are difficult to produce in a reproducible manner. Furthermore, the compositions of the alloys and the thermomechanical processing required to achieve optimal performance requires the establishment of special production facilities, which would be economically viable only if Al/air batteries came into widespread use because of either a shortage of petroleum fuels for ICEs or severe limitations placed on the burning of fossil fuels for environmental reasons.

An attractive alternative to alloy fuels is the possible use of solution-phase inhibitors to reduce the corrosion rate of an aluminum anode to an acceptable level. In this case, it

might be possible to use scrap aluminum as fuel, in which case the cost of the fuel might have been partly or wholly defrayed by previous use. Furthermore, special alloying and thermomechanical processing facilities would not be required, because the anodes could be simply cast from the melted scrap. Solution-phase inhibition has been explored briefly in the past,[1,2] with the result that stannate has been added to the alkaline electrolyte of various experimental aluminum/air batteries. However, no systematic studies of solution-phase inhibition have been reported.

In this report, we present an evaluation of various inorganic oxyanions [SnO_3^{2-}, $Ga(OH)_4^-$, $In(OH)_3$, MnO_4^{2-}, BiO_3^{3-}, and combinations thereof] as inhibitors for the corrosion of pure aluminum (99.99%) in 4 M KOH at 50°C. These ions were chosen because they are derived from metals that have been explored previously[22] as alloying additions and have been shown to influence the rate of corrosion of the alloy. We also report studies on cycling Alloy BDW (Al-1Mg-0.1 In-0.2Mn) between the active and passive states in 4 M KOH at 50°C. This alloy was developed by ALCAN as a potential fuel for Al/air batteries and has exhibited good performance, at least in laboratory tests. The cycling studies were performed to determine the response of the alloy to simulated multiple stop-start cycles such as might be experienced in an actual vehicle.

As a continuation of our previous work[22-25] on the mechanisms of dissolution of aluminum and aluminum alloys in alkaline media, we have explored the effect of hydroxide concentration on the delineated metal dissolution and hydrogen evolution partial reactions as a function of applied potential. These studies were intended to be of a preliminary nature to determine the feasibility of measuring kinetic orders of the partial reactions with respect to hydroxide ion. However, the data also have a practical application in that the concentration of hydroxide ion decreases as an Al/air battery is discharged according to the overall cell reaction

$$4Al + 3O_2 + 6H_2O + 4OH^- \rightarrow 4\,Al(OH)_4^- \qquad (1)$$

and it is possible that superior performance might be achieved by employing an alkaline solution of different concentration than that currently used.

Finally, we have continued our theoretical studies of the electrochemical impedance properties of aluminum alloys in alkaline media. We have been able to account for the negative resistance observed[26] at low frequencies for Al-Ga-In-Tl alloys in 4 M KOH at 25°C, 50°C, and 60°C in terms of a primitive passivation model. As expected, neither the experimental data nor the impedance calculated from the model for potentials at which

negative resistance is observed obeys the Kramers-Kronig transforms.[27] This is an important finding that may have profound implications for the application of electrochemical impedance spectroscopy (EIS) in the study of electrochemical systems.

During this one year program, we had originally proposed to continue our previous systematic studies of aluminum alloy fuels. The proposed work required the availability of carefully prepared alloys containing alloying additions of Mg, In, Mn, and Ga so that the role of each element could be explored. The original intent was that the alloys would be prepared elsewhere in the aluminum/air battery program, because insufficient funds had been allocated to the present study to cover the necessary preparative work. However, a suitable supplier apparently could not be located, so the effort scheduled for the alloy work was rescheduled to expand the solution- phase inhibition work.

EXPERIMENTAL

APPARATUS

The electrochemical cell used to study the effects of solution- phase inhibition on aluminum is shown in Figure 1. The cell is made from clear polyvinyl chloride (PVC) sections bolted together to form a unit about 10 cm long that comprises both a test section and a monitoring section. The cell is placed in a flow loop (Figure 2) with the electrolyte entering the test section at a flow rate of 0.35 gal/min via a PTFE piston pump (Cole-Parmer Model 7149-10). The electrolyte reservoir is immersed into a constant temperature bath set at $50 \pm 1°C$. A calibrated thermocouple measures the temperature at the entrance to the test cell.

The working electrode for the test section consists of a 99.99% aluminum disk (3 mm long and 6 mm in diameter) connected to a thin aluminum rod with silver conducting epoxy (Ecobond). The sides of the disk and the epoxied connection are coated with Amercoat to minimize crevice corrosion. After drying, the specimen is mounted in Quickmount, an acrylic resin, and threaded to fit the working electrode port on the test cell. The exposed aluminum surface area is 0.283 cm^2. Figure 2a shows the epoxy-encapsulated aluminum working electrode on the right-hand side.

The counter electrode is a nickel rod situated in a chamber opposite the aluminum disk but separated from the flow channel by a Nafion-901 membrane. A Hg/HgO reference electrode contacts the electrolyte through a port at the bottom of the flow channel (Figure 2a). The reference electrode is maintained at the cell temperature, to avoid any thermal junction contribution to the measured potential. Data for converting the potentials to the standard hydrogen scale are available from our previous work.[28]

The function of the monitoring section is to measure the rate of hydrogen evolution at the aluminum disk working electrode.[23] This is done by oxidizing the dissolved hydrogen in a porous collector electrode, which was fabricated from monolithic reticulated nickel (Figure 2b). To ensure fast kinetics for the oxidation of hydrogen, we platinized the nickel foam at regular intervals, as previously described.[23] The monitoring section is equipped with a separate Hg/HgO reference electrode and a nickel counter electrode for

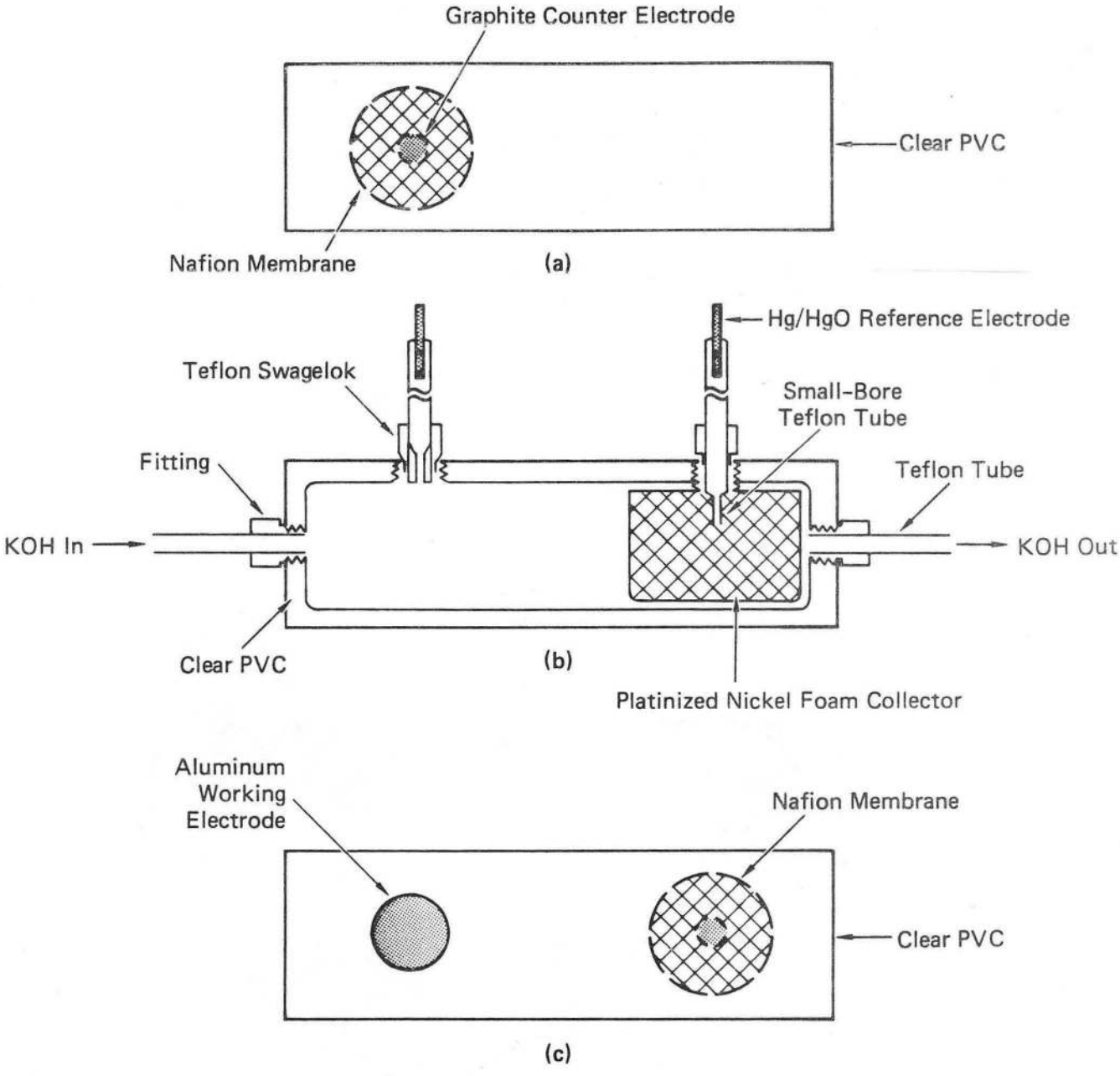

NOTE: Outer sections (a) and (c) are bolted to inner section (b)

Figure 1. Sections of electrochemical cell for polarization measurements of aluminum alloys.

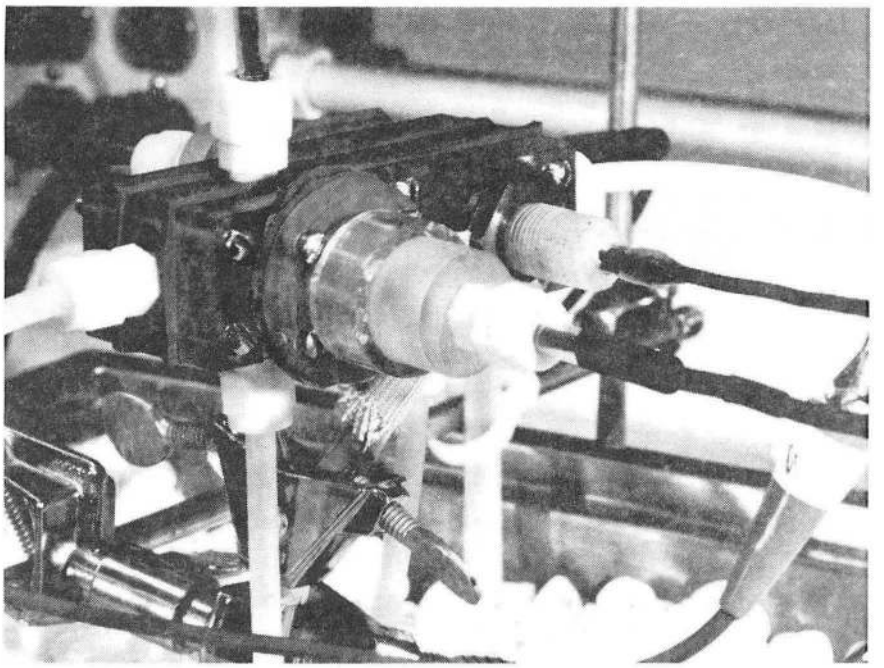

(a)

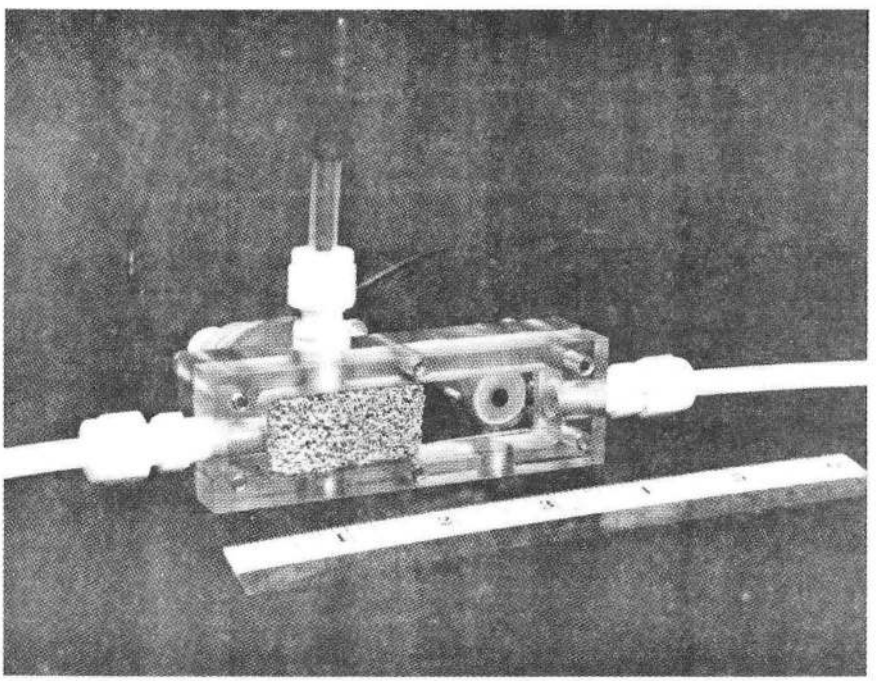

(b)

Figure 2. Electrochemical cell.

(a) View of cell placed in flow loop

(b) Section of the electrochemical cell showing the platinized nickel foam collector electrode

potentiostatic control. The counter electrode chamber for the collector electrode is shown on the left-hand side of Figure 2a. The entire test system is shown in Figure 3.

This test cell design permitted study of the electrodissolution of aluminum and the effects of solution-phase inhibitors while simultaneously allowing separation of the anodic and cathodic partial currents that occur at the interface.

SOLUTIONS

Inhibitor solutions of varying compositions were prepared in Analytical Reagent grade KOH (4 M) using deionized and distilled water. Total solution volume for each experiment was 400 mLs; a fresh solution was prepared for each test. When solutions were changed between experiments, a residual amount of solution (~25 mL) always remained in the pump reservoir. Accordingly, the system was flushed a minimum of five times with 4 M KOH to insure thorough removal of the previous solution. This residual volume results in an error in the final concentration values of the inhibitors (but not of the KOH), but it was not accounted for because of the difficulty of draining the pump reservoir after each experiment. However, we estimate that the error never exceeds 7%, and an acceptable correction can be applied if necessary. A dilute H_2SO_4 (0.01 M) rinse was periodically flushed through the loop as a general cleansing agent; this was followed by a water rinse and several KOH rinses.

All compounds except $Ga(OH)_3$ and K_2MnO_4 were commercially available. $Ga(OH)_3$ was prepared by dissolving 5 g of gallium (III) nitrate hydrate [$Ga(NO_3)$-3.9 H_2O, 99.9%] in 100 mLs of deionized and distilled water and titrating to a pH of 7.6 with KOH. The resultant fine precipitate was separated from the solvent by centrifugation, washed three times with distilled water, and then dried in an oven overnight at 75°C.

Potassium manganate (K_2MnO_4) was prepared by adding 10 g of $KMnO_4$ to 30 g of KOH in 50 ml of water and boiling until a clear green solution was obtained. The flask was then set in ice until a precipitate formed. The black-green crystals were collected by filtration, washed with 1 M KOH, and dried.[29]

Gallium and indium were added as the hydroxide species [$Ga(OH)_3$ and $In(OH)_3$] and Bi, Sn, and Mn were added as the oxyacid salts ($NaBiO_3$, Na_2SnO_3, and K_2MnO_4, respectively). All compounds readily dissolved in 4 M KOH, with the exception of $In(OH)_3$, which required heating for dissolution to occur.

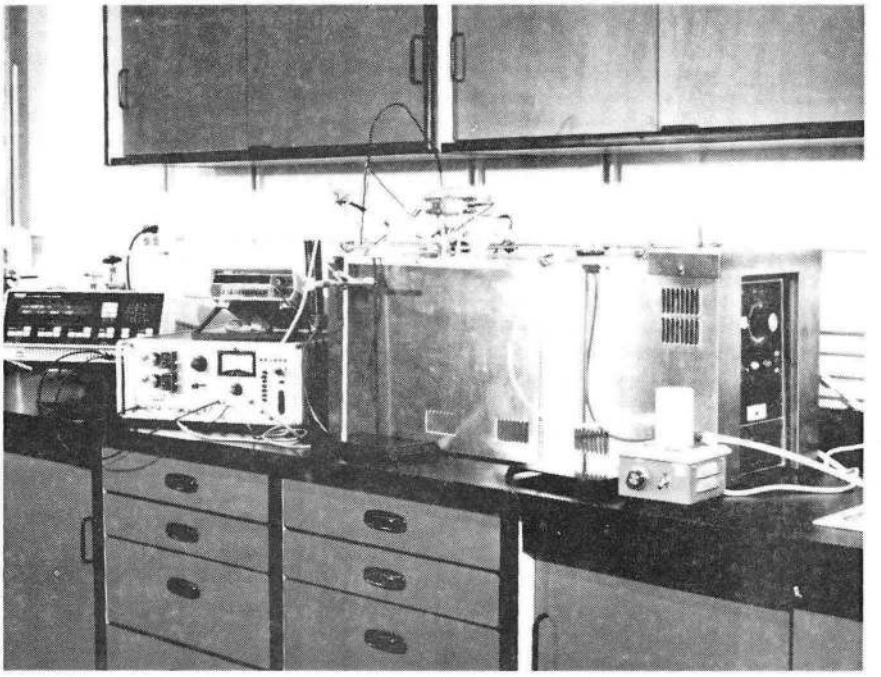

Figure 3. General view of the experimental apparatus and electrochemical cell.

EXPERIMENTAL TECHNIQUE

Before each experiment, the aluminum electrode surface was polished with 400- and 600-grit SiC paper and then by 0.3- and 0.05- μm alumina powder on microcloth. The surface was thoroughly rinsed with deionized water, then with ethanol, and finally with deionized and distilled water. The working electrodes were placed in a beaker of deionized and distilled water and sonicated for approximately two minutes to remove any residual particles from the surface. A new aluminum specimen was used for each experiment.

The electrolyte was placed in the reservoir and allowed to equilibrate at 50° ± 1°C for a minimum of one hour before an experiment while simultaneously being sparged with nitrogen at a flow rate of 4 scfh. The solution was continuously sparged for the duration of the experiment to prevent buildup of hydrogen in the system. At the end of the equilibration period, the Al working electrode was inserted into the test cell and equilibrated under open circuit conditions for another hour. A potential of -0.5 V was applied (Thompson Electrochem Microstat) to the monitoring section during this time. The final open circuit potential of the aluminum specimen was recorded at the end of this period.

The recorded open circuit potential was applied to the test specimen using an EG&G Model 362 potentiostat and then slowly decreased (to prevent overload) to -2000 mV (vs Hg/HgO, 4 M KOH). The potential was then increased in a stepwise manner in the positive direction, and current readings were taken after each 25-mV increment. The currents from the test section and from the monitoring section were allowed to stabilize and then were read as voltage drops across standard resistors. The stabilization time varied from run to run, but was usually between 10 and 30 minutes. The potential range over which the measurements were obtained was -2.0 to -1.2 V (vs Hg/HgO, 4 M KOH) as established in our previous work.[23,24]

RESULTS

DISSOLUTION OF ALUMINUM IN 4 M KOH

Duplicate delineated current/voltage curves for aluminum in 4 M KOH at 50°C are shown in Figure 4. These plots demonstrate the reproducibility that was achieved in this work, which was generally within ±10% for the current at any given potential provided that the experiments were performed in an identical manner.

As we observed previously[23,24] aluminum is a passive metal in 4 M KOH at 50°C. This passivity is clearly shown in Figure 4 by the existence of a passive region in which the current is nearly independent of potential (-1.9 V to -1.65 V), as well as by the tail end of an active-to-passive transition (-2.0V to -1.95V). At voltages more positive than -1.65 V, the current increases nearly linearly with potential, which indicates the existence of a transpassive film of constant (potential-independent) resistance. In this respect, aluminum resembles zinc in alkaline environments,[30] although we have not observed the current oscillations in the Al/OH^- system that are characteristic of the Zn/OH^- system at high potentials.

We recently[25] developed a kinetic model for the electrochemistry of aluminum in KOH solutions, that accounts very well for the impedance characteristics over a wide range of applied potential and frequency. The essence of this model is that aluminum electrodissolution occurs via the stepwise addition of hydroxide ions to reactive centers and ultimately results in a fully coordinated surface species, $Al(OH)_3$, which then dissolves chemically as $Al(OH)_4^-$. The electrodissolution mechanism is coupled to hydrogen evolution (which is significant over the entire potential range of interest - see Figure 4) by competition for surface sites. In the simulations of the impedance data,[25] we had to assume that the surface concentration of active sites varied in a manner paralleling the anodic current (iA) shown in Figure 4. Furthermore, the concentration (mol/cm^2) required for the simulation corresponds to many monolayers, which suggests that the surface is covered by a porous macroscopic film over the entire potential range of interest. The picture which emerges is that the surface is covered by a porous film whose porosity mimicks the anodic current/voltage curve and that the passivating reactions involving the stepwise adsorption of OH^- occur at the base of the pores. The existence of a macroscopic

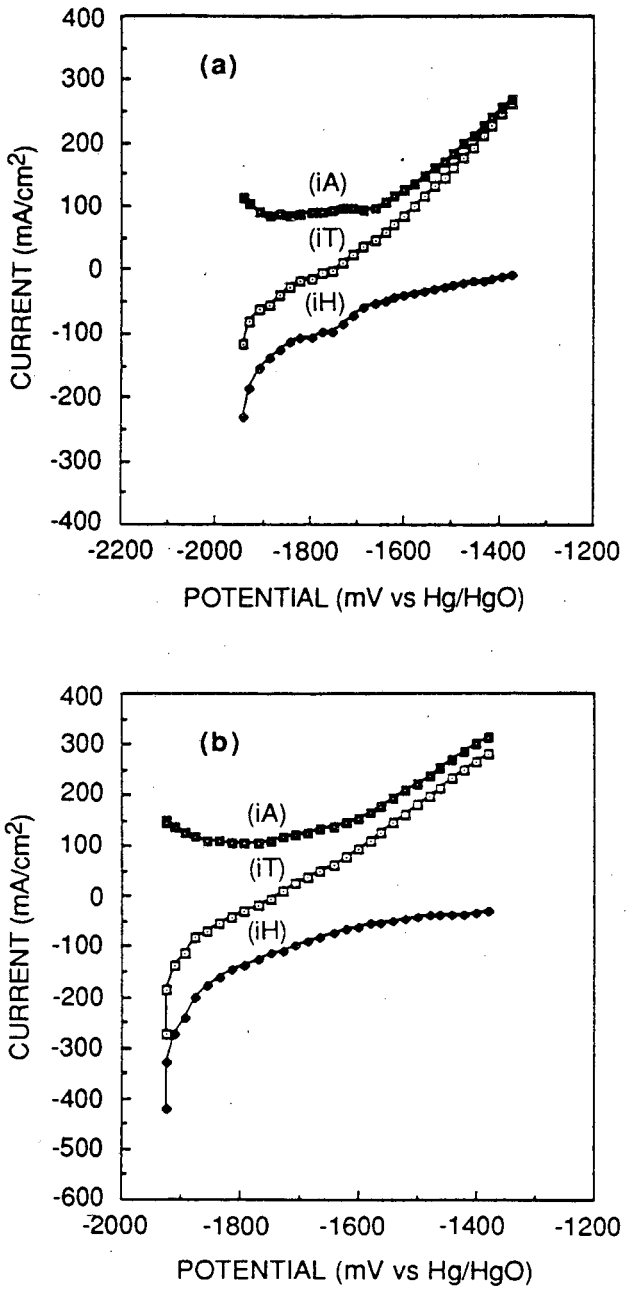

Figure 4. Duplicate steady-state polarization curves [(a) and (b)] for pure aluminum in KOH at 50° C, showing the total current (iT) and both anodic (iA) and cathodic (iH) partial currents.

hydroxide/oxide film on aluminum in alkaline environments has been detected by a number of workers.[31-33]

The concentration of hydroxide ion in the solution was found to have a strong effect on the electrochemical behavior of aluminum in KOH, as shown in Figures 4 and 5. At low (1 M) hydroxide concentrations (Figure 5a), both the hydrogen partial reaction and the aluminum electrodissolution reaction are independent of potential over a wide range of voltage, from -1.85 V to -1.1 V. Although the total current is small, the anodic dissolution partial current is large (~100 mA/cm^2) and is of the same order as that observed in the passive region for a higher (4 M) KOH concentration (Figure 4). Indeed, the region of potential-independent current observed in Figure 5a corresponds to a greatly expanded passive region that was originally detected in the 4 M KOH solution in our previous work.[23] At a still higher KOH concentration (Figure 5b), the passive region is considerably reduced, with the onset of transpassive dissolution being detected at -1.8 V. The transition to the transpassive state is accompanied by a marked increase in the rate of hydrogen evolution and hence in the rate of corrosion of the metal under discharge conditions.

The effect of hydroxide concentration on the electrodissolution of aluminum is shown more explicitly by comparing the anodic partial current/voltage curves in Figure 6. Clearly, [OH^-] has an enormous effect on the dissolution behavior of aluminum in the transpassive region, with the current at any given potential increasing strongly with increasing hydroxide concentration. On the other hand, the reverse is observed in the passive region, particularly when the hydroxide concentration is increased from 4 M to 8 M (Figure 6). In this case, the passive current is found to decrease to a very small value (< 10 mA/cm^2) at potentials more negative than -1.82 V.

The data contained in Figures 4 to 6 show that hydroxide ion inhibits aluminum electrodissolution in the passive range but catalyzes the reaction in the transpassive region. Although the data are not extensive enough to provide a detailed mechanistic explanation of these phenomena, our findings have important practical implications for aluminum/air battery technology. Thus, provided that hydrogen evolution in the transpassive region can be inhibited by the addition of suitable alloying elements to the metal, considerable advantages may exist in operating Al/air batteries at very high KOH concentrations. With these high KOH concentrations, advantage can be taken of the lower corrosion current under standby and the faster kinetics of discharge in the transpassive region.

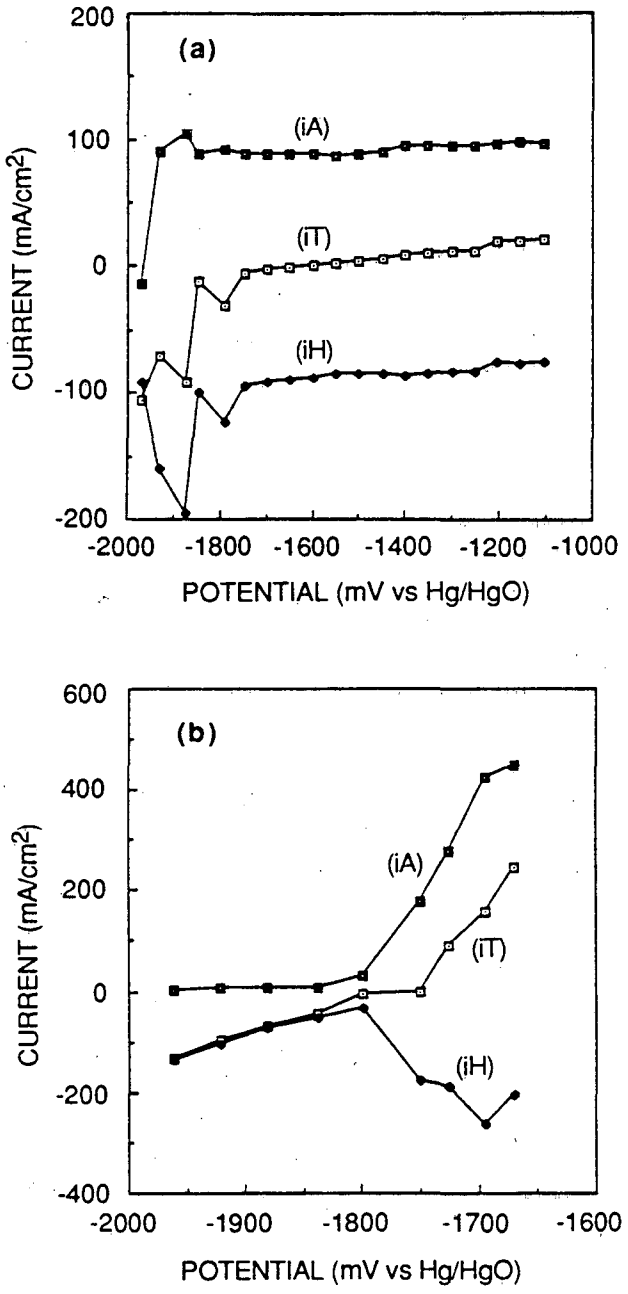

Figure 5. Steady-state polarization curves for pure aluminum in KOH at 50° C, showing the total current (iT) and both anodic (iA) and cathodic (iH) partial currents.

(a) [KOH] = 1M
(b) [KOH] = 8M

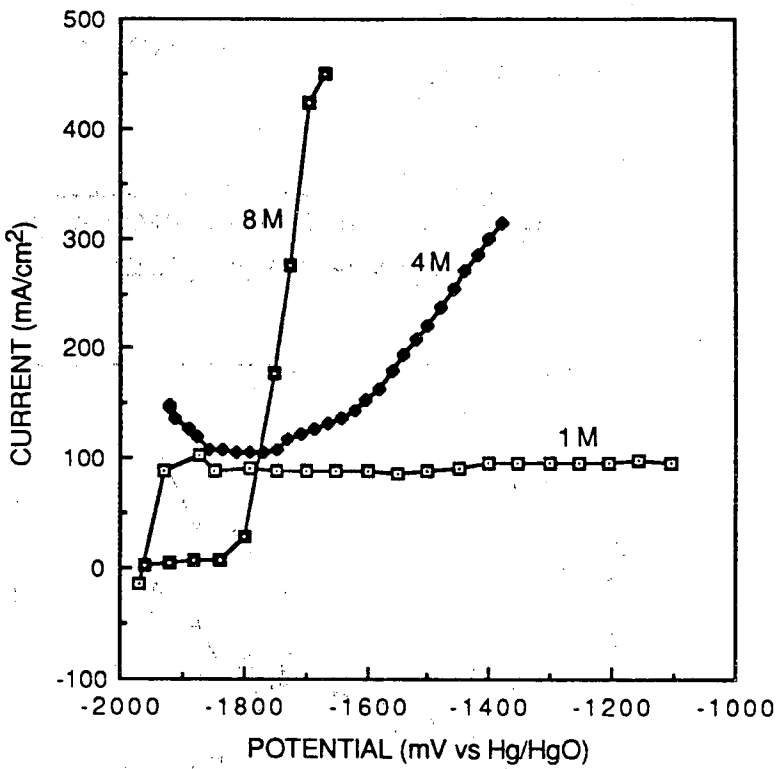

Figure 6. Comparison of the partial anodic curves for aluminum in 1 M, 4 M, and 8 M KOH at 50° C.

SOLUTION-PHASE INHIBITION

Aluminum showed significantly less reproducibility of current/voltage curves in the presence of various solution-phase inhibitors than in the presence of uninhibited solutions, as shown by comparing Figure 4 with Figures 7 and 8. Nevertheless, the data were sufficiently reproducible that important trends could be discerned as a function of inhibitor type and concentration. In this project, we were especially concerned with the mechanism of inhibition, in particular whether the inhibitor affected the partial anodic reaction, the cathodic reaction, or both. Our goal was to identify solution-phase inhibitors that kinetically hinder the cathodic reaction alone, because such inhibitors would have the effect of reducing the open circuit corrosion rate without affecting the discharge characteristics. Also, cathodic inhibition alone causes the open circuit potential (OCP) to be displaced in the negative direction and thus results in an apparent increase in the power density of the anode. This latter effect is an illusion because it is the power density under discharge, which is dominated by the partial anodic reaction, that is the important characteristic of the fuel.

Single-Component Inhibitor Systems

Stannate. Previous studies have shown that stannate ion (SnO_3^{2-}) inhibits the corrosion of aluminum in hydroxide solutions, and early work of Cooper et al.[1,2] and others[34] employed this species to inhibit fuel corrosion in aluminum/air test cells. However, to our knowledge, the only studies on the mechanism of inhibition have been the brief impedance studies of Macdonald et al.[35] who concluded that SnO_3^{2-} is reduced to metallic tin to form a porous deposit on the surface.

Our current work (Figure 7) demonstrates that stannate addition inhibits both the anodic and cathodic partial reactions at the open circuit potential with the former dominating at very high concentrations (Figure 7c). These observations are consistent with the reduction of SnO_3^{2-} by the more electronegative aluminum to form a porous metallic deposit on the surface. At high (positive) potentials for the most concentrated stannate solution (Figure 7c), the current is observed to increase sharply with increasing potential. The increase in current cannot be due to oxidation of the deposited tin, because the potential at which this process could occur is far more positive (-1.13 V vs Hg/HgO, 4 M KOH[36]). Instead, the mechanism probably involves undermining of the deposited tin by aluminum dissolution, which ultimately leads to decohesion of the deposit from the surface. The

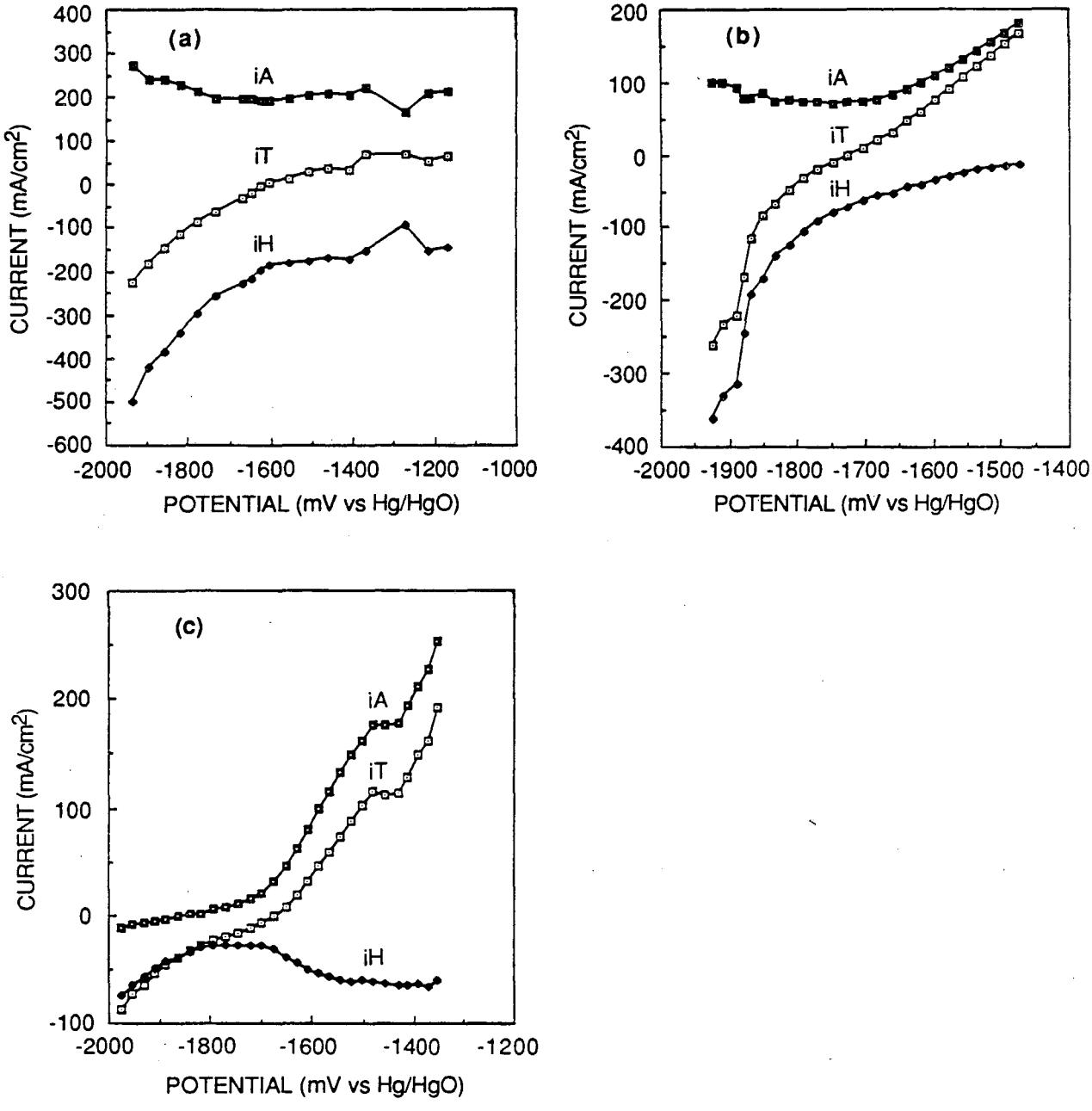

Figure 7. Steady-state polarization curves for pure aluminum in x M Na_2SnO_3 + 4 M KOH at 50°C, showing the total current (iT) and both anodic (iA) and cathodic (iH) partial currents.

(a) x = 10^{-4} M
(b) x = 10^{-3} M
(c) x = 10^{-2} M

experiments with stannate always resulted in the formation of colloidal tin suspended in the aqueous phase.

The explanation offered above is supported by the behavior of the hydrogen evolution current. Thus, as the potential is made more positive (E > -1.7 V), the cathodic current increases to ultimately match that observed for the stannate-free system (Figure 4). The increase in the hydrogen evolution current implies an increase in corrosion rate under discharge conditions, which can only lead to a lower efficiency of anode utilization. For this reason, we do not consider stannate alone to be a viable solution-phase inhibitor system for practical aluminum/air batteries.

Gallium. Gallium is an important component of many alloys that have been investigated as potential fuels for alkaline aluminum/air batteries. Accordingly, there has been considerable interest in studying the effect of $Ga(OH)_4^-$ on the electrodissolution of aluminum in alkaline media.

Typical plots of the delineated anodic and cathodic currents versus potential are shown in Figure 8. The first notable feature is that the anodic and cathodic currents at very negative potentials (E < -1.9 V) are extraodinarily high (>10^4 mA/cm^2), while the apparent curent (iT) remains close to zero. These data show that the corrosion reaction dominates the chemistry of the interface, to such an extent that the aluminum specimen was completely consumed upon completion of an experiment. Indeed, the decrease in the anodic and cathodic currents with increasing potential shown in Figure 8 is an experimental artifact that is due to the complete consumption of the anode by the time the potential exceeded -1.8 V (note that the potential was increased in 25-mV steps in the positive direction). After the anode was consumed, both the observed current (iT) and the hydrogen evolution current (iH) would register zero, which would cause the calculated current for aluminum dissolution also to be zero. These results clearly demonstrate the nonviability of gallate as a solution-phase inhibitor.

Indium. Indium is also a common alloying element in the development of alloy anodes for alkaline aluminum/air batteries and, in fact, is an important alloying component of Alloy BDW (Al-1Mg-0.1In-0.2Mn), which has received so much attention over the past few years. Delineated current/voltage curves for aluminum in 4 M KOH with various concentrations of $In(OH)_3$ are shown in Figure 9. At all concentrations, a sharp increase occurs in both the anodic and cathodic partial currents as the potential is increased from the passive zone in the positive direction. At still higher potentials, the surface passivates, with the result that there is a sudden decrease in both iA and iH to values that are typical of

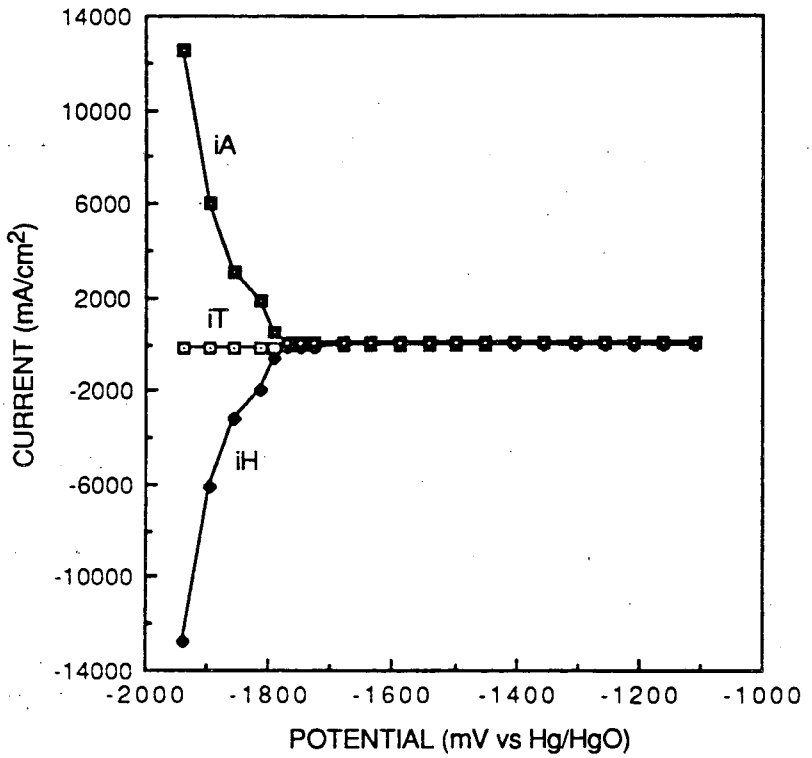

Figure 8. Steady-state polarization curves for pure aluminum in 1×10^{-3} M $Ga(OH)_3$ + 4 M KOH at 50° C, showing the total current (iT) and both anodic (iA) and cathodic (iH) partial currents.

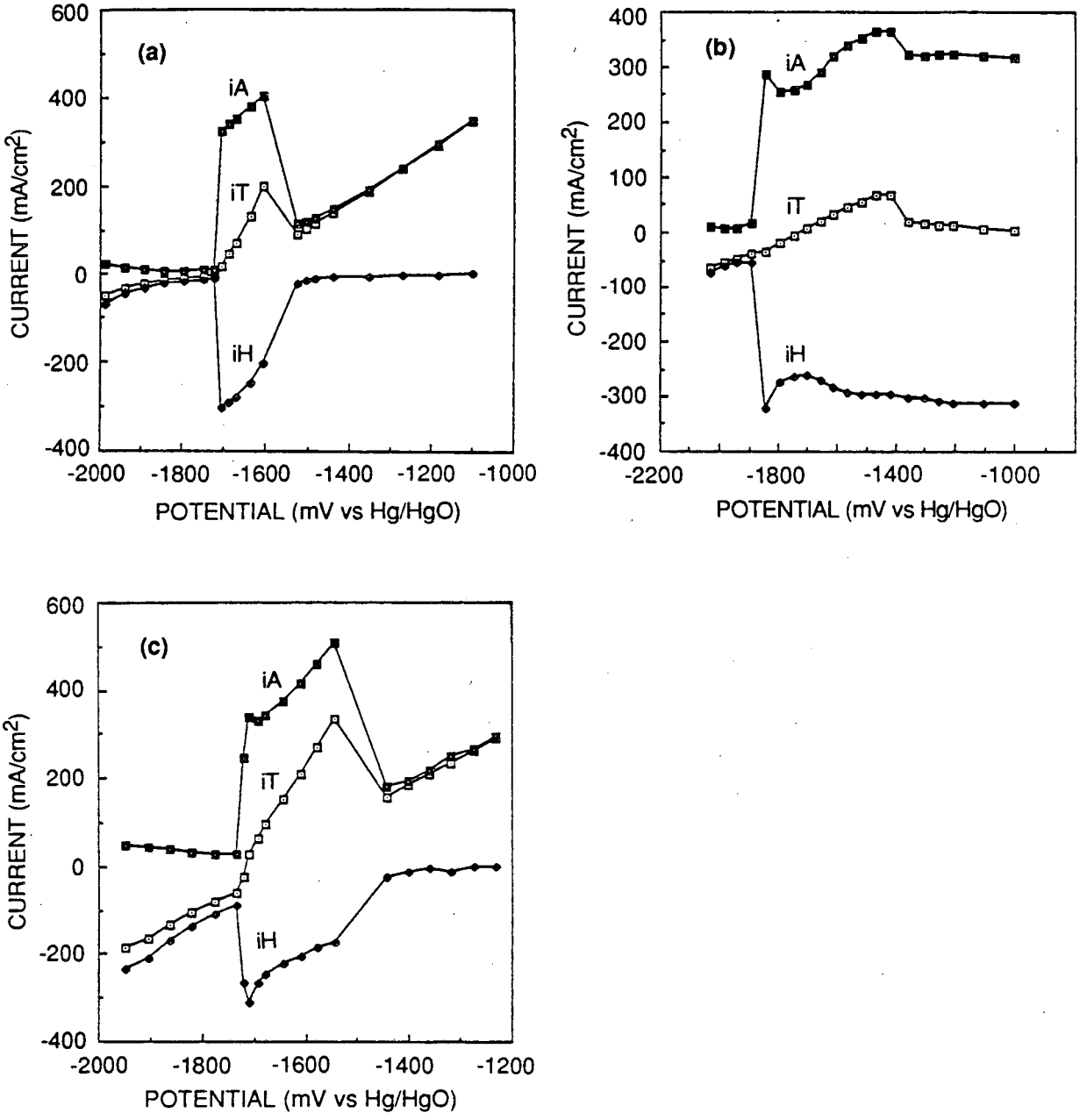

Figure 9. Steady-state polarization curves for pure aluminum in x M $In(OH)_3$ + 4 M KOH at 50° C, showing the total current (iT) and both anodic (iA) and cathodic (iH)partial currents.

(a) x = 10^{-4} M
(b) x = 10^{-3} M
(c) x = 10^{-2} M

aluminum in pure 4 M KOH (Figure 4). These observations strongly suggest that indium interferes with the normal passivating reactions on the aluminum surface, possibly by forming a deposit of metallic indium. This explanation is viable if we assume that hydrogen evolution is a much faster reaction on indium than it is on passive aluminum and thereby supports a greatly enhanced aluminum dissolution current in the presence of the metallic indium film. As the potential is made still more positive, the indium film becomes unstable, presumably because of undercutting of the aluminum as in the case of stannate. At sufficiently positive potentials (E > -1.5 V), the deposited indium is removed from the surface and the surface reactions are characteristic of those that occur on aluminum alone. Note that the equilibrium potential for $In/In(OH)_3$ is ~ -1.10 V(vs. Hg/HgO, 4 M KOH),[36] so oxidative removal of indium from the surface does not appear to be a viable explanation for the decrease in iA and iH that occurs at high potentials. The existence of high corrosion currents at intermediate potentials renders $In(OH)_3$ alone unsuitable as a solution-phase inhibitor.

Manganese. Alloy BDW (Al-1Mg-0.1In-0.2Mn) contains manganese as an alloying element in addition to indium and magnesium. The lowest oxyanion of manganese (ignoring the possible existence of $Mn(OH)_3^-$) is manganate (MnO_4^{2-}), in which the manganese atom is in the +6 oxidation state. The equilibrium potentials[36] for the Mn/MnO_4^{2-} (10^{-3} M) and MnO_2/MnO_4^{2-} couples in 4 M KOH at 50°C are estimated from thermodynamic data[15] to be approximately -0.49 V and + 0.34 V (vs Hg/HgO), respectively, so manganate might be expected to be reduced to insoluble products (Mn or MnO_2) and hence act as an effective inhibitor of aluminum corrosion in alkaline media. However, these same data suggest that activation by oxidation of Mn or MnO_2 to MnO_4^{2-} will not occur at potentials of interest in this work although activation by the formation of $HMnO_2^-$ is possible because the equilibrium potential for the $Mn/HMnO_2^-$ couple is estimated to be about -1.7 V (vs Hg/HgO).

Typical delineated current/voltage curves for aluminum in 10^{-3} M K_2MnO_4 + 4 M KOH and 10^{-2} M K_2MnO_4 + 4 M KOH solutions at 50°C are shown in Figure 10. At potentials more positive than -1.7 V, the hydrogen evolution current is greatly reduced (especially for the lowest K_2MnO_4 concentration) and the observed current (iT) is due almost entirely to alloy dissolution. Comparison of Figures 4 and 10 indicates that some inhibition of the anodic current occurs, as would be expected if a thin layer of reaction product (possibly MnO_2) exists at the surface, but comparison of manganate with stannate for equivalent concentrations (Figure 7) indicates that manganate is a more effective solution-phase inhibitor for aluminum/air battery applications, particularly at low

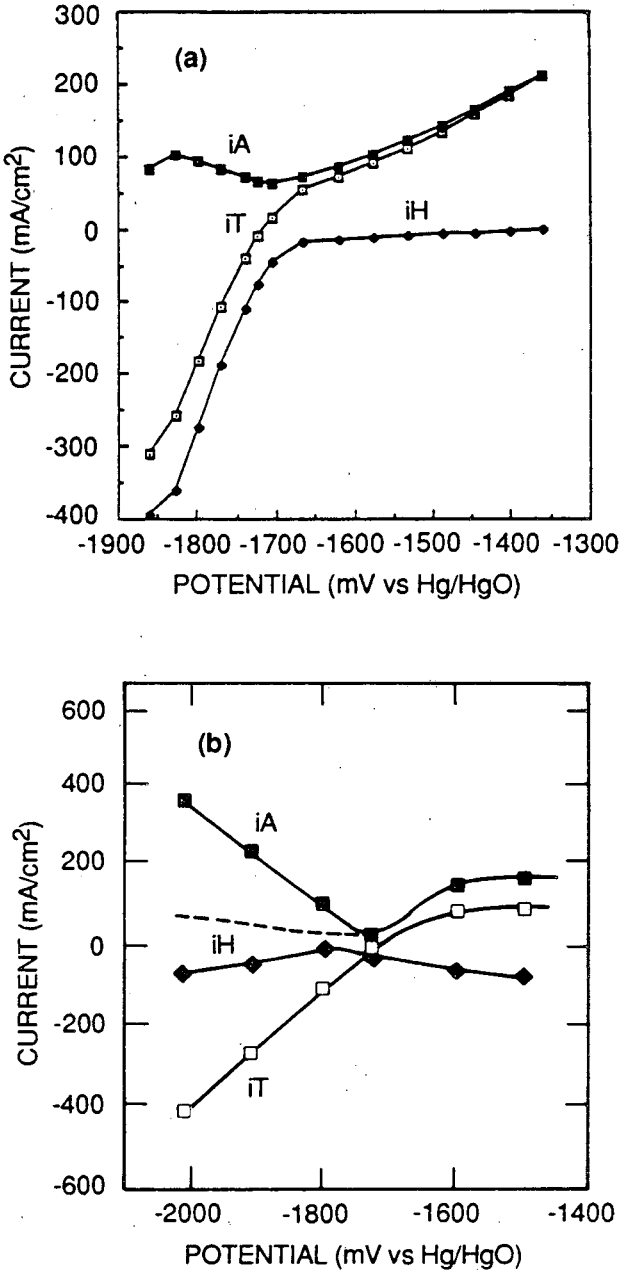

Figure 10. Steady-state polarization curves for pure aluminum in x M K_2MnO_4 + 4 M KOH at 50° C, showing the total current (iT) and both anodic (iA) and cathodic (iH) partial currents.

(a) x = 10^{-3}
(b) x = 10^{-2}

- - - Corrected anodic dissolution current (iA)

concentrations (e.g.,10^{-3} M). Indeed, the effectiveness of manganate in inhibiting hydrogen evolution is such that it should be evaluated in aluminum/air test cells.

The data in Figure 10b for the highest K_2MnO_4 concentration investigated in this work, show that for potentials more negative than -1.75 V the total current (i.e., that observed in the external circuit) is more negative than the hydrogen evolution current. A similar phenomenon is observed in the case of stannate solutions (Figure 7c), although to a much smaller extent. This phenomenon coincides with a gradual change in the color of the solution from green (MnO_4^-) to light brown (MnO_2). The color change results from the reaction

$$MnO_4^{2-} + 2H_2O + 2e^- \rightarrow MnO_2 + 4OH^- \qquad (2)$$

which occurs in parallel with hydrogen evolution to form colloidal MnO_2 (brown). Reaction (2) also accounts for the additional cathodic reaction that results in the reversal of the relative magnitudes of iH and iT depicted in Figure 10b. It is important to note that the electrodissolution current (iA) is calculated from iH and iT, with the assumption that hydrogen evolution is the only cathodic reaction occurring at the surface. Accordingly, the iA values indicated in Figure 10b for potentials in the cathodic region are artifactually too high. Noting that iT in the absence of Reaction (2) can never be more negative than iH, we place a probable upper limit on iA indicated by the broken line in Figure 10b.

Bismuth is also an element that showed some promise[22,34] as an alloying component for alloy fuels for aluminum/air batterires, but it has proven to be completely ineffective as a solution-phase inhibitor (Figure 11).

Multi-Component Inhibitor Systems

Our previous studies on the corrosion of aluminum alloys in alkaline media[22] demonstrated a synergistic effect between alloying elements in inhibiting hydrogen evolution, so it was of interest to determine whether these same effects occur in solution-phase inhibition.

$Ga(OH)_4^-$ + $In(OH)_3$. A combination of $Ga(OH)_4^-$ and $In(OH)_3$ is clearly ineffective as an inhibitor system because of the exceedingly high hydrogen evolution currents observed at potentials more positive than -1.5 V (Figure 12a). Clearly, this combination of solution-phase species destroys the passivity of aluminum, to such an extent that the hydrogen evolution current very quickly reaches the maximum that can be

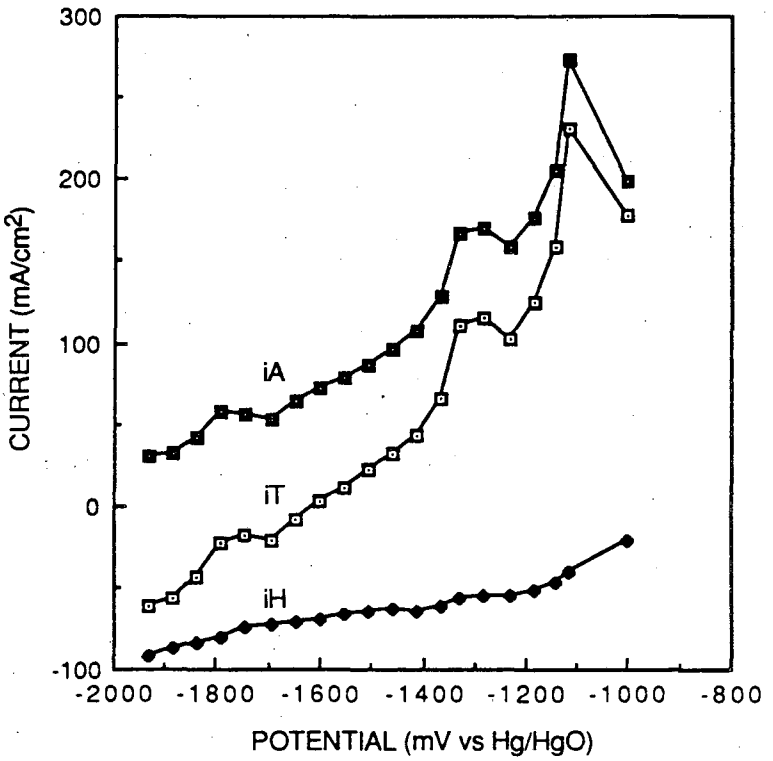

Figure 11. Steady-state polarizaton curves for pure aluminum in 1 x 10^{-3} M K_2MnO_4 + 4 M KOH at 50° C, showing the total current (iT) and both anodic (iA) and cathodic (iH) partial currents.

detected by the collector electrode. At these potentials, the specimen quickly dissolved. Similar results were obtained at a lower $Ga(OH)_4^-$ concentration (10^{-4} M), but at 10^{-5} M $Ga(OH)_4^-$ (+10^{-3} M $In(OH)_3$), the massive corrosion of the substrate evident in Figure 12a did not occur. These observations are of considerable interest because Al-Ga-In was found in our previous work[22-24] to be a promising alloy fuel.

K_2MnO_4 + $In(OH)_3$. Inhibitor systems containing K_2MnO_4 + $In(OH)_3$ were also investigated because of the promising characteristics of Alloy BDW. At moderate concentrations of both components, the delineated current/voltage curves (Figure 12b) are similar to those displayed by aluminum in the manganate solution alone (Figure 10a), except that the currents are of greater magnitude in the multicomponent system. Further additions of $In(OH)_3$ increased the hydrogen evolution current still further, so that in solutions of [$In(OH)_3$] >10^{-2} M, the beneficial effect of MnO_4^- was no longer evident.

$NaBiO_3$ + Na_2SnO_3. Solutions containing 10^{-3} M $NaBiO_3$ + 10^{-2} M Na_2SnO_3 also displayed unexpected behavior (Figure 12c); in this case the hydrogen evolution current was found to be essentially independent of potential (as detected by the collector electrode) over a wide range of potential, which resulted in the anodic dissolution partial current tracking the total current. At potentials more negative than -1.7 V, the anodic current became large and negative, presumably because of the reduction of stannate, bismuthate, or both at the surface. However, the hydrogen evolution current was still substantial (30-50 mA/cm^2), so BiO_3^- + SnO_3^{2-} is not considered to be a viable inhibitor system.

SnO_3^{2-} + $In(OH)_3$. The final multicomponent inhibitor system investigated in this work was SnO_3^{2-} + $In(OH)_3$. As shown in Figure 13, this system results in moderate hydrogen evolution currents (5-25 mA/cm^2) for E > E_{OCP} while allowing high discharge (dissolution) currents at reasonably negative voltages (iA = 600 mA/cm^2 at -1.45 V). A passivation event at -1.45 to -1.35 V resembles that observed for Alloy BDW.[24] However, unlike the case for Alloy BDW, no concomitant response is observed in the hydrogen evolution current. When the $In(OH)_3$ concentration was decreased, the passivation event was no longer observed and there was a substantial decrease in the anodic partial current at any given potential. Clearly, $In(OH)_3$ has an activating effect on the dissolution of aluminum in this medium, but the expected increase in the hydrogen evolution current (compare with Figure 9) is effectively countered by the stannate addition. The Na_2SnO_3 + $In(OH)_3$ system must be considered highly promising for practical aluminum/air batteries.

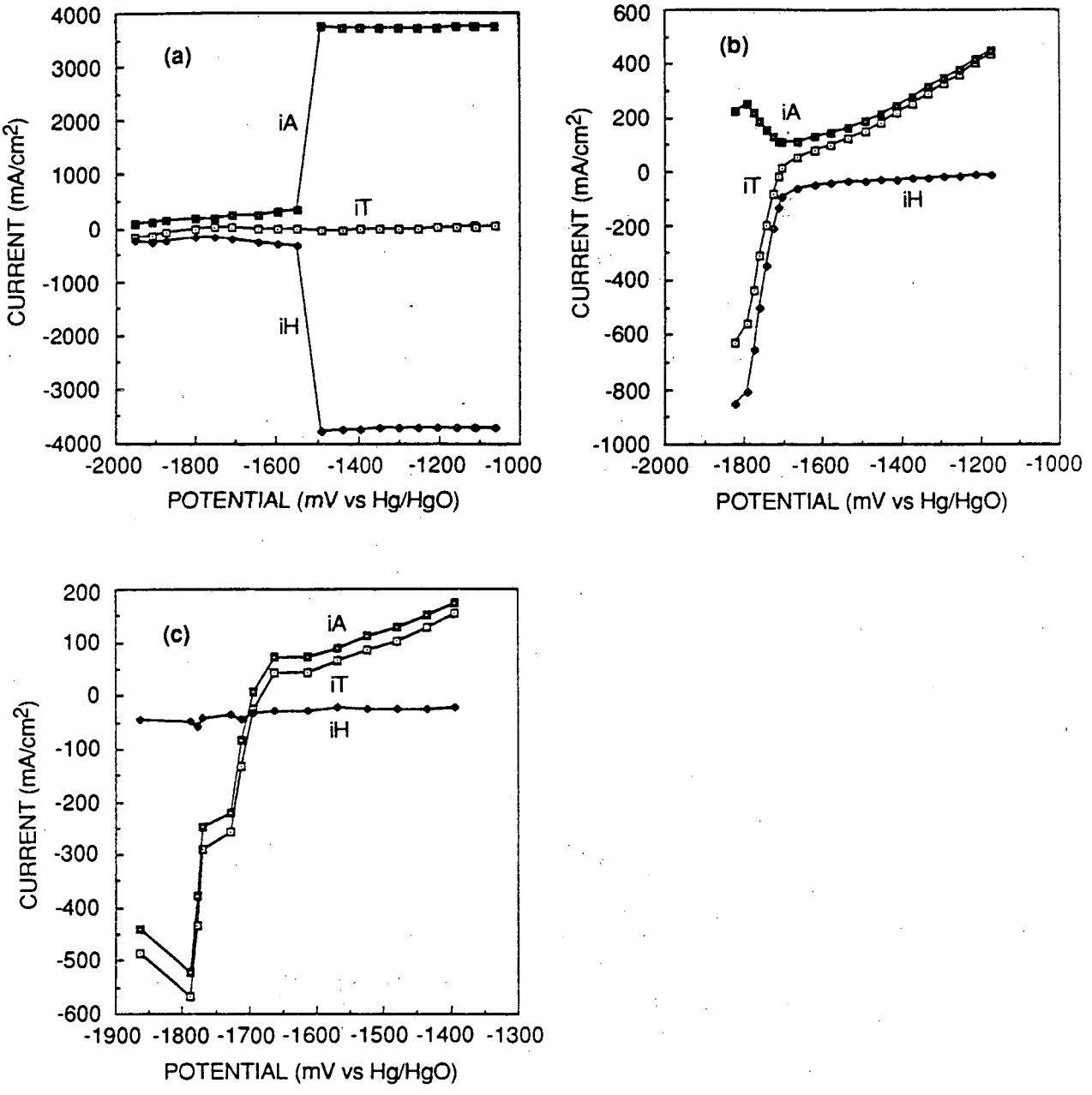

Figure 12. Steady-state polarization curves for pure aluminum in x + 4 M KOH at 50° C, showing the total current (iT) and both anodic (iA) and cathodic (iH) partial currents.

(a) x = 10^{-3} M $Ga(OH)_3$ + 10^{-3} M $In(OH)_3$
(b) x = 10^{-3} M K_2MnO_4 + 10^{-3} M $In(OH)_3$
(c) x = 10^{-3} M $NaBiO_3$ + 10^{-2} M Na_2SnO_3

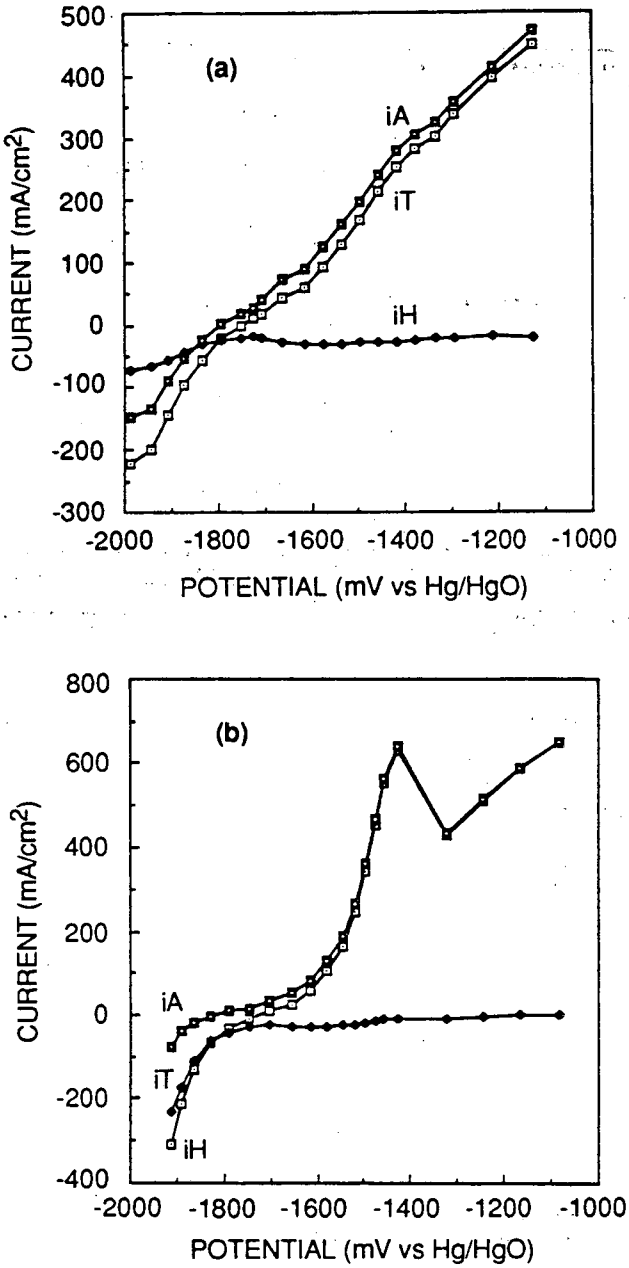

Figure 13. Steady-state polarization curves for pure aluminum in 10^{-2} M Na_2SnO_3 +x M $In(OH)_3$ + 4 M KOH at 50° C, showing the total current (iT) and both anodic (iA) and cathodic (iH) partial currents.

(a) x = 10^{-3}
(b) x = 10^{-2}

Cycling of Alloy BDW

Our previous work[24,26] and that of others[34] have shown ALCAN's Alloy BDW (Al-1 Mg-0.1 In-0.2 Mn) to be a promising candidate as a fuel for Al/air batteries. Only alloys containing thallium were found to exhibit superior electrochemical characteristics,[24] but the presence of Tl renders these alloys unacceptable from an environmental viewpoint. In operation, the anode must be capable of cycling between the standby and discharge states without any significant degradation of coulombic efficiency. To our knowledge, this aspect of alloy performance has not been investigated previously, but it is clearly a matter of considerable importance in the development of practical batteries.

To address this issue, we performed multiple (sequential) determinations of the polarization behavior of Alloy BDW in 4 M KOH at 50°C. Four cycles are shown in Figure 14. The absence of significant changes over these cycles indicates that progressive surface roughening and perhaps dealloying do not occur to significant extents.

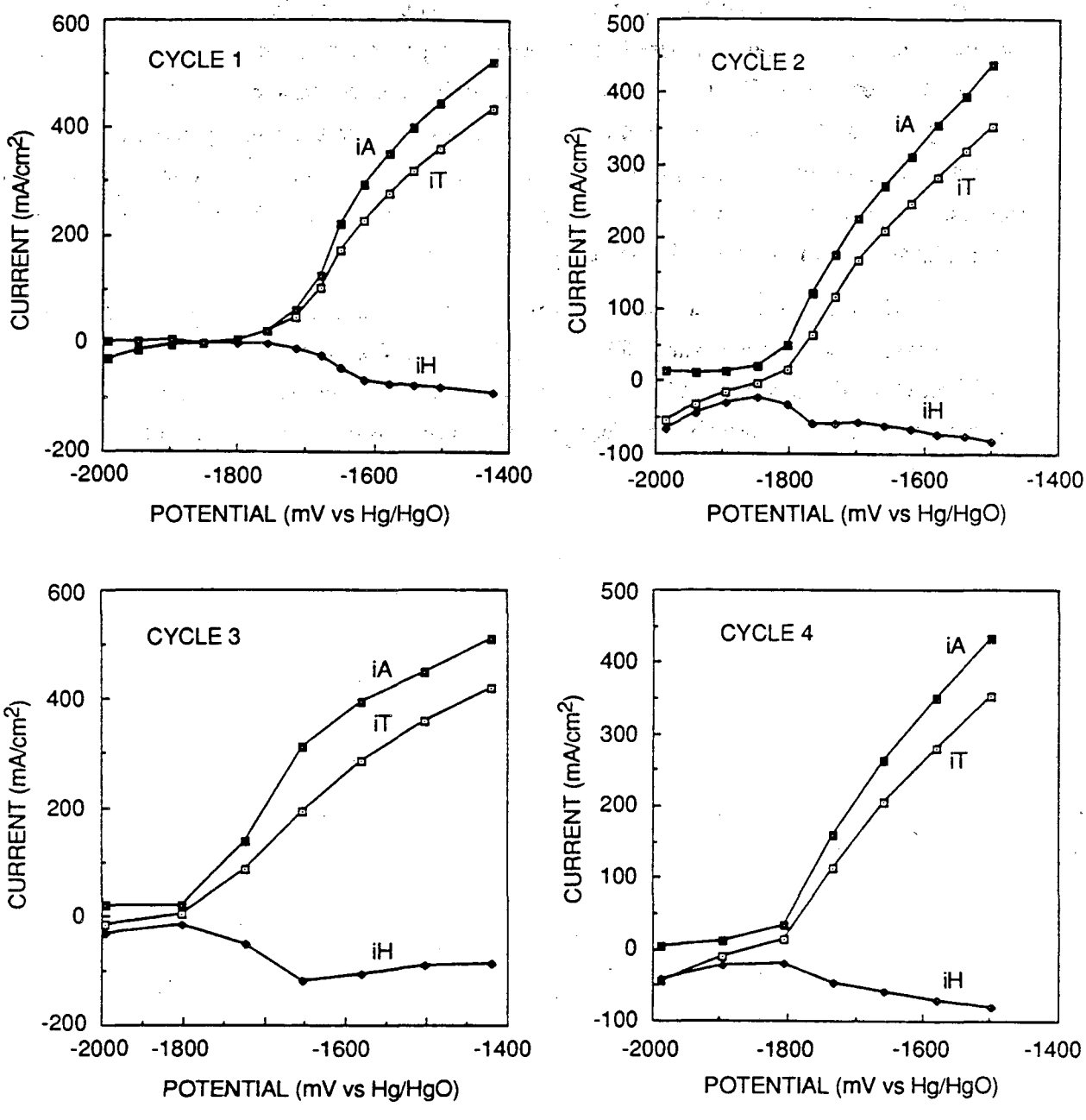

Figure 14. Steady-state polarization curves for Alloy BDW in 4 M KOH at 50° C, showing the total current (iT) and both anodic (iA) and cathodic (iH) partial currents as a function of cycle number.

DISCUSSION

When assessing the performances of fuels for aluminum/air batteries, we are concerned with three parameters: the open circuit corrosion rate (i_{corr}^{ocp}), and the discharge voltage (E_D) and corrosion rate (i_{corr}^{D}) under a given load. The open circuit corrosion rate determines the loss of fuel (self discharge) during standby, and hence should be kept as low as possible. However, a moderately high open circuit corrosion rate might be tolerated in practice if the battery was drained during standby. The discharge voltage (E_D) and the corrosion rate (i_{corr}^{D}) under load (iT) are important because they define the operating characteristics of the fuel; the product $P_D = |E_D \cdot iT|$ is a measure of the power density (mW/cm^2) of the fuel, and $CE = iT/(iT + i_{corr}^{D})$ is a measure of the coulombic efficiency with which the fuel is used as the battery is being discharged. A superior fuel will have high values for both quantities.

Open circuit corrosion potentials (E_{corr}), open circuit corrosion rates (i_{corr}^{ocp}), and discharge parameters (E_D, i_{corr}^{D} at various discharge currents) for aluminum, Alloy BDW, and Alloy 21 in alkaline and inhibited alkaline environments are summarized in Table 1. These data have been used to calculate the relative open circuit corrosion rates and the values for the power density (P_D) and coulombic efficiency (CE) listed in Table 2.

Not all of the "inhibitors" investigated in this work reduced the corrosion rate of aluminum below that for aluminum in 4 M KOH. For example, with the addition of $In(OH)_3$, the corrosion rate increased by almost a factor of three (Tables 1 and 2) under open circuit conditions and to much higher values under discharge conditions, with the result that coulombic efficiencies for fuel utilization were low (Table 2). The ability of $In(OH)_3$ to destroy the passivity of aluminum is clearly evident from the current/voltage curves shown in Figure 9. A similar but much more intense effect was observed when $Ga(OH)_3$ was added to the electrolyte (Figure 8); its result was complete destruction of the aluminum specimen.

Stannate ion (SnO_3^{2-}), when present at high concentrations, caused a substantial decrease in the open circuit corrosion current but still produced poor coulombic efficiency under discharge compared with that in the uninhibited environment. In fact, for a Na_2SnO_3 concentration of 10^{-3} M, the coulombic efficiency for a net discharge current of 200

Table 1.

PERFORMANCE DATA FOR ALUMINUM AND ALUMINUM ALLOYS IN ALKALINE AND INHIBITED ALKALINE SOLUTIONS AT 50°C.

Alloy	Solution (+ 4M KOH)	E_{corr} (V vs. Hg/HgO)	i^{ocp}_{corr} (mA/cm^2)	E_D(V vs Hg/HgO) + (i^D_{corr}(mA/cm^2)) at iT of 100 mA/cm^2	200 mA/cm^2	400 mA/cm^2
Al	-	-1.71	95	-1.56 (43)	-1.41 (24)	-
Al	10^{-3} M Na_2SnO_3	-1.73	72	-1.54 (26)	-1.44 (10)	-
Al	10^{-2} M Na_2SnO_3	-1.68	31	-1.48 (59)	-1.30 (60)	-
Al	10^{-3} M $In(OH)_3$	-1.74	264	-	-	-
Al	10^{-2} M $In(OH)_3$	-1.73	280	-1.65 (235)	-1.55 (206)	-
Al	10^{-3} M K_2MNO_4	-1.73	65	-1.50 (9.6)	-1.30 (2.0)	-
Al	10^{-3} M K_2MnO_4 + 10^{-3} M $In(OH)_3$	-1.71	100	-1.55 (42)	-1.32 (29)	-1.10 (15)
Al	10^{-3} M K_2MnO_4 + 10^{-2} M $In(OH)_3$	-1.70	70	-1.40 (44)	-1.10 (30)	-
Al	10^{-2} M Na_2SnO_3 + 10^{-3} M $In(OH)_3$	-1.72	19	-1.55 (31)	-1.40 (27)	-1.10 (18)
Al	10^{-2} M Na_2SnO_3 + 10^{-2} M $In(OH)_3$	-1.75	26	-1.55 (27)	-1.47 (24)	-1.38 (17)
BDW (Al-1Mg-0.1In-0.2Mn)		-1.80	5	-1.65 (25)	-1.57 (60)	-1.46 (80)
21 (Al-0.2Ga-0.1In-0.1Tl)		-1.64	4.6	-1.35 (<1)	-	-

Table 2.

POWER DENSITIES AND COULOMBIC EFFICIENCIES FOR ALUMINUM AND ALUMINUM ALLOYS IN ALKALINE AND INHIBITED ALKALINE SOLUTIONS AT 50°C.

Alloy	Solution	$(i^{o}_{corr}/i^{ocp}_{corr}(Al)$	P_D and (CE) at a Discharge Current of 100 mA/cm^2	200 mA/cm^2	400 mA/cm^2
Al	-	1	156 (0.70)	282 (0.89)	ND
Al	10^{-3} M Na_2SnO_3	0.76	154 (0.79)	288 (0.95)	ND
Al	10^{-2} M Na_2SnO_3	0.33	148 (0.63)	260 (0.77)	ND
Al	10^{-3} M $In(OH)_3$	2.78	NA*	NA	NA
Al	10^{-2} M $In(OH)_3$	2.95	165 (0.30)	310 (0.49)	NA
Al	10^{-3} M K_2MnO_4	0.68	150 (0.91)	260 (0.99)	ND
Al	10^{-3} M K_2MnO_4 + 10^{-3} M $In(OH)_3$	1.05	155((0.70)	264 (0.87)	440 (0.96)
Al	10^{-3} M K_2MnO_4 + 10^{-2} M $In(OH)_3$	0.74	140 (0.69)	220 (0.87)	ND
Al	10^{-2} M Na_2SnO_3 + 10^{-3} M $In(OH)_3$	0.20	155 (0.76)	280 (0.88)	440 (0.96)
Al	10^{-2} M Na_2SnO_3 + 10^{-2} M $In(OH)_3$	0.27	155 (0.79)	294 (0.89)	552 (0.96)
BDW (Al-1Mg-0.1In-0.2Mn)		0.05	165 (0.80)	314 (0.77)	584 (0.83)
21 (Al-0.2Ga-0.1In-0.1Tl)		0.048	135 (>0.99)	ND*	ND

*NA = Not achieved. ND = Not determined.

mA/cm^2 was found to be 95%, whereas that for [Na_2SnO_3] = 10^{-2} M under similar conditions was only 77% and that for discharge at a net current of 100 mA/cm^2 was 79%. The inhibitive effect of stannate ion on aluminum corrosion under open circuit conditions has been documented (by Cooper et al.[1,2]), but its effect on the coulombic efficiency of aluminum in hydroxide media under discharge conditions had previously not been characterized.

Of the single-component inhibitor systems explored in this work, that containing potassium manganate (K_2MnO_4) was the most effective. At a concentration of 10^{-3} M, which is considered to be practical in operating batteries, the coulombic efficiency of the aluminum anode was found to exceed 90% for discharge currents of 100 mA/cm^2 and 200 mA/cm^2, with the efficiency for the highest discharge rate being 99%. However, the open circuit current was less than a factor of two smaller than that of the inhibitor-free system (Table 2).

For the four binary inhibitor systems listed in Table 2, the best performance was displayed by the stannate + indium hydroxide systems, which yield open circuit corrosion rates lower by factors of four to five than those of the uninhibited solutions and display coulombic efficiencies as high as 96% for a net discharge current of 400 mA/cm^2. Indeed, the coulombic efficiencies exhibited by these systems at the two highest discharge rates (200 and 400 mA/cm^2) are substantially higher than those observed for Alloy BDW, which is a leading candidate fuel for aluminum/air batteries, but only marginally better than those for aluminum in uninhibited 4 M KOH. Clearly, the only benefit of the inhibitors in these cases is suppression of the open circuit corrosion rate. Alloy BDW exhibits a much lower open circuit corrosion rate than does aluminum in either the inhibited or uninhibited environments, but the coulombic efficiency performance of Alloy BDW under discharge is not substantially better than that of aluminum, which indicates that alloying benefits only the standby performance in this particular case. Only Alloy 21, the thallium containing alloy, matches Alloy BDW in its standby corrosion characteristics (Table 2), but the discharge voltage for Alloy 21 is significantly more positive (and hence the power density is lower) than that for Alloy BDW. Insufficient data are available to determine the coulombic efficiency of Alloy 21 under high rate discharge ($iT \geq 200$ mA/cm^2) conditions, but extrapolation of the data contained in Reference 24 indicates that the coulombic efficiency would be very high (essentially equal to 100%).

Finally, the data listed in Table 2 show that Alloy BDW exhibits the highest power densities of any system at all discharge rates considered in this work, because of the more negative discharge voltages exhibited by this alloy. However, our previous work[24]

indicated that Alloy BDW may exhibit a secondary passivation phenomenon at high potentials, in which case the power density approaches that for pure aluminum.

SUMMARY AND CONCLUSIONS

The discharge characteristics of aluminum in 4 M KOH and in inhibited 4 M KOH solutions at 50°C have been explored. We found that potassium manganate (K_2MnO_4) and Na_2SnO_3 + $In(OH)_3$ are effective inhibitor systems, particularly at high discharge rates (400 mA/cm^2), but at low discharge rates only manganate offers a significant advantage in coulombic efficiency over that of the uninhibited solution. Alloy BDW exhibits a very low open circuit (standby) corrosion rate, but its coulombic efficiency under discharge was found to be no better than that of aluminum in the same uninhibited solution. Alloy 21, however, exhibited a performance comparable to that of Alloy BDW under open circuit conditions and a much higher coulombic efficiency at low discharge rate (100 mA/cm^2) conditions. The performance of Alloy 21 under high discharge rate conditions was not determined. Alloy 21 has the significant disadvantage that it contains thallium.

REFERENCES

1. J. F. Cooper, R. V. Homsky, and J. H. Landrum, "The Aluminum-Air Battery for Electric Vehicle Propulsion," in *Proceedings of the 15th Intersociety Energy Conversion Engineering Conference, June 1980*, (Lawrence Livermore National Laboratory UCRL-84443, Livermore, California, 1980).

2. J. F. Cooper, R. V. Homsy, J. H. Landrum, and S. P. Perone, "The Mechanically-Refuelable Aluminum-Air Battery," in *Proceedings of the 15th Intersociety Energy Conversion Engineering Conference, June 1980,* Lawrence Livermore National Laboratory UCRL-84443, Livermore, California, 1980).

3. S. P. Perone, N. Kirkman Bey, and J. F. Cooper, "Parametric Study of an Alkaline-Electrolyte Aluminum-Air Flow Cell," *Proceedings of the 15th Intersociety Energy Conversion Engineering Conference, June 1980*, Lawrence Livermore National Laboratory UCRL-84443, Livermore, California, 1980.

4. J. D. Salisbury, E. Behrin, M. K. Kong, and D. J. Whisler, "A Comparative Analysis of Aluminum-Air Battery Propulsion Systems for Passenger Vehicles," Lawrence Livermore National Laboratory, UCRL-52933, Livermore, California, February 1980.

5. "Aluminum-Air Battery System, Assessment of Technical and Market Viability for Electric Vehicle Application," Final Report to Brookhaven National Laboratory, Alvin J. Salkind Associates, December 1980.

6. "Control System Considerations for an Aluminum-Air Battery Powered Electric Vehicle," Final Report to Lawrence Livermore National Laboratory, William M. Brobeck and Associates, May 1980.

7. A. R. Despic, *Recueil Des Travaux*, **12** (No. 1), 1(1979).

8. H. B. Urgach and M. C. Cervi, "Aluminum-Based Anodes for Underwater Fuel Cells," *Proceedings of the 12th Intersociety Energy Conversion Engineering Conference* No. 1, p. 276, 1977.

9. W. A. Bryant and E. S. Buzzelli, "A Comparison of Metal-Air Batteries for Electric Vehicle Propulsion," Proceedings ot the 14th Intersociety Intersoc. Energy Conversion Engineering Conference, No. 1, pp. 651-653, 1979.

10. J. F. Cooper, "Preliminary Design and Analysis of Aluminum-Air Cells Providing for Continuous Feed and Full Utilization of Anodes," DOE Report 1981, UCID0-19178, Order No. DE81030479, p. 9, 1981.

11. R. V. Homsy, "Rapidly-Refuelable 167 cm^2 Aluminum-Air Power Cell," DOE Report 1981, UCID-19244; Order No. DE82006251, p. 44, 1981.

12. O. R. Brown and J. S. Whitley, *Electrochim. Acta.*, **32**, 545 (1987).

13. Y. Hori, J. Takaom and H. Shomon, *Electrochim. Acta.*, **30**, 1121 (1985).

14. F. Dalard, J. Y. Macht, J. Guilton, and J. C. Sohm, *Electrochim. Acta*, **21**, 249, (1976).

15. W. Bohnstedt, *J. Power Sources*, **5**, 245, (1980).

16. W. Schneider and K. Wiesner, *Bull. Chem. Soc. Beeg.*, **48**, 5241, (1983).

17. C. J. McMinn and J. A. Branscomb, "Production of Anodes for Aluminum-Air Power Cells Directly from Hall Cell Metal," Report to DOE, Subcontract No. 6124909 (1981).

18. A. R. Despic, D. M. Drazic, M. M. Purenovic, and N. Cikovic, *J. Appl. Electrochem.*, **6**, 527 (1976).

19. J. R. Moden and G. Perkons, U.S. Patent No. 4,150,104 (1979).

20. A. R. Despic, D. M. Drazic, M. M. Purenovic, and N. Cikovic, *J. Appl. Electrochem.*, **6**, 527 (1976).

21. S. Zecevic, L. Gajic, A. R. Despic, and D. M. Drazic, *Electrochim. Acta*, **26**, 1625 (1981).

22. D. D. Macdonald, K. H. Lee, A. Moccari, and D. Harrington, *Corrosion*, **44**, 652 (1988).

23. S. Real, M. Urquidi-Macdonald, and D. D. Macdonald, *J. Electrochem. Soc.*, **135**, 2397 (1988).

24. D. D. Macdonald, S. Real, and M. Urquidi-Macdonald, J. Electrochem. Soc., 135, 1633 (1988).

25. D. D. Macdonald, S. Real, S. I. Smedley, and M. Urquidi-Macdonald, *J. Electrochem. Soc.*, **135**, 2410 (1988).

26. D. D. Macdonald, S. Real, S. I. Smedley, and M. Urquidi-Macdonald, "Development and Evaluation of Anode Alloys for Aluminum-Air Batteries," Final Report to Eltech Systems Corp., DOE Subcontract 100484-MLM, 1987.

27. M. Urquidi-Macdonald, S. Real, and D. D. Macdonald, *J. Electrochem. Soc.*, **133**, 2018 (1986).

28. B. G. Pound, R. P. Singh, and D. D. Macdonald, *J. Power Sources*, **18**, 1 (1986).

29. K. A. Jensen and W. Klemm, *Z. Anorg. Allg. Chem.*, **237**, 47 (1938).

30. M.C.H. McKubre and D. D. Macdonald, J. Electrochem. Soc., 127, 632 (1980).

31. K. E. Heusler and W. Allgaier, *Werkst. Korros.*, **22**, 297 (1971).

32. O. R. Brown and J. S. Whitley, *Electrochim. Acta*, **32**, 545 (1987).

33. R. Greef and C.F.W. Norman, *J. Electrochem. Soc.*, **132**, 2362 (1985).

34. Eltech Systems Corp., private communication, 1987.

35. D. D. Macdonald, K-H. Lee, A. Moccari, D. Harrington, and M. Urquidi, "The Metallurgy and Electrochemistry of the Aluminum Anode," Final Report to ELTECH Systems Corp. from Ohio State University, FCC 5162, May 10, 1984.

36. M. Pourbaix, *Atlas of Electrochemical Equilibria*, (National Association of Corrosion Engineers Eng., Houston, TX ,1974).

Appendix I

Papers Submitted or Published During the Contract Period

1. D. D. Macdonald, K. H. Lee, A. Moccari, and D. Harrington, "Evaluation of Alloy Anodes for Aluminum-Air Batteries: Corrosion Studies," *Corrosion*, **44**, 652-7 (1988).

2. S. Real, M. Urquidi-Macdonald, and D. D. Macdonald, "Evaluation of Alloy Anodes for Aluminum-Air Batteries. II Delineation of Anodic and Cathodic Partial Reactions," *J. Electrochem. Soc.*, **135**, 1633 (1988).

3. D. D. Macdonald, S. Real, and M. Urquidi-Macdonald, "Evaluation of Alloy Anodes for Aluminum-Air Batteries. III Mechanisms of Activation, Passivation, and Hydrogen Evolution," *J. Electrochem. Soc.*, **135**, 2397-2409 (1988).

4. D. D. Macdonald, S. Real, S. I. Smedley, and M. Urquidi-Macdonald, "Evaluation of Alloy Anodes for Aluminum-Air Batteries. IV Electrochemical Impedance Analysis of Pure Aluminum in 4 M KOH at 25°C," *J. Electrochem. Soc.*, **135**, 2410-4 (1988).

5. D. D. Macdonald, M. Urquidi-Macdonald, and R. Rocha-Filho, "Kramers-Kronig Transforms of Systems that Exhibit Negative Resistance" (to be submitted to *J. Electrochem.*, 1989).

6. D. D. Macdonald and Catherine English, "Evaluation of Alloy Anodes for Aluminum-Air Batteries. V Solution Phase Inhibition of Aluminum Corrosion," (to be submitted to *Corrosion*, 1989).

LAWRENCE BERKELEY LABORATORY
TECHNICAL INFORMATION DEPARTMENT
1 CYCLOTRON ROAD
BERKELEY, CALIFORNIA 94720